ELSEVIER

Journal of Structural Geology 27 (2005) 1838–1855

JOURNAL OF STRUCTURAL GEOLOGY

www.elsevier.com/locate/jsg

Propagation of strike-slip faults across Holocene volcano-sedimentary deposits, Pasto, Colombia

Andrea Rovida*, Alessandro Tibaldi

Dipartimento di Scienze Geologiche e Geotecnologie, Università di Milano-Bicocca, Piazza della Scienza, 4-20126 Milano, Italy

Received 1 April 2004; received in revised form 9 June 2005; accepted 17 June 2005
Available online 19 August 2005

Abstract

This study contributes to the understanding of shear failure development on the basis of macroscopic field data collected in latest Pleistocene–Holocene pyroclastic and fluvio-lacustrine deposits in the Pasto Valley, SW Colombia. Here there is a pervasive system of microfaults and joints. Right-lateral strike-slip microfaults strike N065°, whereas left-lateral strike-slip microfaults strike N120°. Three main joint sets strike N, N065° and N020° in decreasing order of frequency. Stress computation gives a horizontal σ_1 trending ~N060° and a horizontal σ_3 trending ~N150°, consistent with earthquake focal mechanisms and stress inversion of main faults. Synthetic shears dominate resulting from nucleation of older cracks. In the basement cropping out northeast of Pasto, the NE- to ENE-striking Buesaco, Aranda and Pasto Faults show evidence of latest Pleistocene–Holocene right-lateral strike-slip motions. The structures in the Pasto Valley can be interpreted as a Mode III damage zone representing the up-dip propagation of the main faults across the young volcano-sedimentary deposits.

Keywords: Strike-slip faults; Faulting processes; Colombia; Quaternary

1. Introduction

The current knowledge about the mechanics of shear failure development derives primarily from experimental data, while there is relatively little published work on the geometry of naturally induced brittle faulting (e.g. Segall and Pollard, 1983; Martel et al., 1988; Willemse et al., 1997). Some previous studies have stressed that shear failure is a localized phenomenon that does not follow a single model, but may rather involve a variety of mechanisms (Rudnicki and Rice, 1975; Willemse et al., 1997).

The volume of deformed wall rocks around a fault surface that results from the initiation, propagation, interaction and build-up of slip along faults is defined as a damage zone (Cowie and Scholz, 1992; McGrath and Davison, 1995), which develops in response to stress concentration at a fault tip. The development of secondary faults and extension fractures in fault zones can play a critical role in fault propagation and growth and can provide information about it (e.g. Cowie and Scholz, 1992; McGrath and Davison, 1995; Kim et al., 2003). Some faults, tens to hundreds of metres long, nucleate along pre-existing joints and grow by subsequent linkage of such sheared joints along Mode I tail cracks, also called wing cracks, splay cracks and pinnate veins (Segall and Pollard, 1983; Hancock, 1985; Hancock and Barka, 1987; Martel et al., 1988; Engelder, 1989; Cruikshank et al., 1991). Various factors, such as lithology, the dip of bedding planes relative to the slip direction of the fault, and the stress system, control the nature of damage zones around faults (Kim et al., 2004). Damage zones around strike-slip faults have been described in detail in recent years (e.g. Segall and Pollard, 1983; Cruikshank et al., 1991; McGrath and Davison, 1995; Martel and Boger, 1998; Kim et al., 2003), and a general account and systematic classification of damage zones are provided by Kim et al. (2004).

The aim of this study is to describe and interpret, using field data, the macro- and meso-scale structural pattern present in the valley of Pasto (southwestern Colombia). The study area represents an exceptional structural situation, in

* Corresponding author. Now at: Instituto Nazionale di Geofisica e Vulcanologia, Sezione di Milano via E. Bassini, 15-20133 Milano, Italy. Tel.: +39 02 23699 272; fax: +39 02 23699 458.
E-mail address: rovida@mi.ingv.it (A. Rovida).

0191-8141/$ - see front matter © 2005 Elsevier Ltd. All rights reserved.
doi:10.1016/j.jsg.2005.06.009

which a complex pattern of Tertiary to Quaternary strike-slip faults affects the basement rocks cropping out to the NE of Pasto while the fault traces seem not to affect the succession of Pleistocene–Holocene volcanic and sedimentary deposits filling the Pasto Valley. On the other hand, in the outcrops in the Pasto Valley, a complex structural pattern of meso-scale faults and fractures has been recognised. Based on the geometric and kinematic features of these structures, they can be interpreted as a Mode III tip damage zone of the strike-slip faults in the basement and, thus, can represent the up-dip propagation of the strike-slip faults from the basement to its cover.

As a result, the study area represents a unique example in which a master strike-slip fault and its Mode III damage zone are both exposed. Moreover, the explosive activity of the Galeras volcano produced a sequence of pyroclastic deposits that accompanied the continuous tectonic activity, recording its progressive stages of development and allowing its interpretation.

After a general description of the geological and tectonic settings, the various types and ages of the structures affecting the recent volcano-sedimentary sequence of the Pasto Valley and surrounding area are documented. Based on these data, we propose a model for the development of

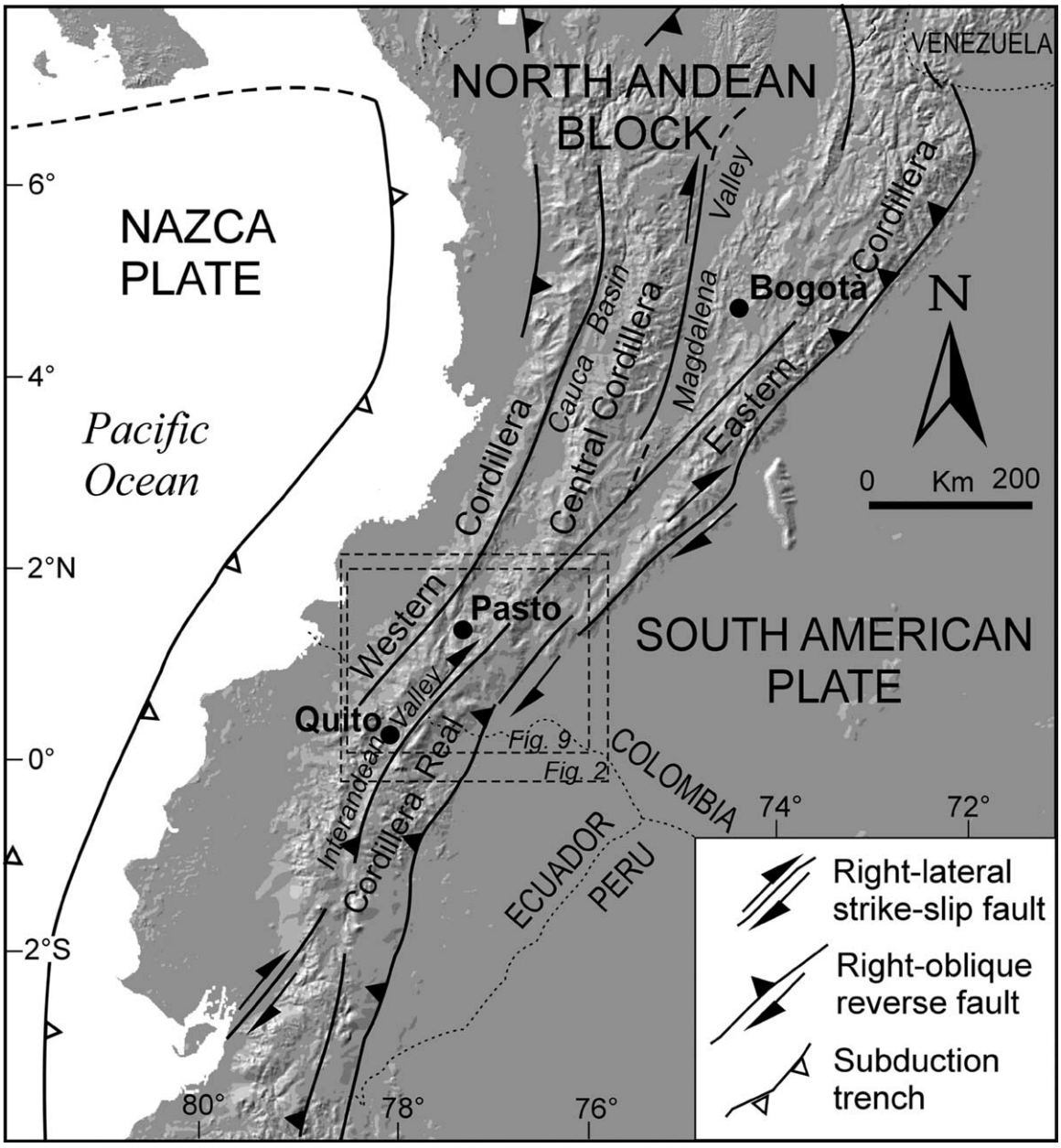

Fig. 1. Physiographic sketch and location of the study area. The study area is located at the transition from the triple cordilleran system of Colombia to the double chain in Ecuador. Boxes locate Figs. 2 and 9.

such a structural pattern. Finally, we comment on the hierarchical evolution of strike-slip fault zones in volcanic rocks, contributing to the understanding of the process of strike-slip fault propagation in volcano-sedimentary deposits.

2. Geology and tectonics of the area

In Colombia, the Andes are composed of three NNE-trending ranges, the Western, Central, and Eastern Cordilleras (Fig. 1), each presenting different geological features (Fig. 2) (Aspden and McCourt, 1986; Paris and Romero, 1994; Kellogg and Vega, 1995). The Romeral Fault System, consisting of NW-dipping reverse and strike-slip NE-striking faults, separates the Western from the Central and Eastern Cordilleras (Figs. 1 and 2) and it is interpreted as a Tertiary suture between the accreted rocks and the continental paleomargin (Case et al., 1973; Duque Caro, 1980; Aspden and McCourt, 1986; Paris and Romero, 1994).

The study area is located in southwestern Colombia, where the three cordilleras merge into the two Ecuadorian chains: the Western Cordillera and the Cordillera Real (Fig. 1). Here, a Pliocene–Pleistocene volcanic succession at least 1 km thick overlies rocks belonging to two different sequences (Fig. 3). To the NW, a sequence of Cretaceous marine metasedimentary and metavolcanic rocks of the Western Cordillera crops out. To the NE and SE, another sequence of Paleozoic metamorphic and Cretaceous–Tertiary intrusive rocks of the Central and Eastern Cordilleras is present. To the SE, metamorphic rocks of Precambrian age crop out. The contact between these sequences is represented by the Cauca-Patia and Romeral Fault Systems, in this area consisting of approximately NE-striking right-lateral strike-slip faults. These rocks are overlain by Tertiary continental sedimentary deposits and Pliocene lavas and pyroclastic rocks in the central and southwestern parts of the study area, which have been grouped in Fig. 3 as 'Tertiary undifferentiated deposits'. Glacial deposits and landforms are present on the southern slope of the Galeras and on Cerro Morazurco, NE of Pasto, down to an altitude of 3400 m.

The valley of Pasto is surrounded to the south and southeast by the remnants of Tertiary volcanoes mainly composed of lavas interlayered with fall deposits, and to the north by the Miocene–Pliocene Morazurco volcano (INGEOMINAS, 1991). To the west, the valley is bounded by the active Galeras volcano (Fig. 5). The valley slopes are generally gentle, the surface being parallel to the dip of pyroclastic fall deposits. The northern slope is steeper due to the presence of extensive lava outcrops related to the Morazurco volcano. The valley floor is flat and the Pasto river runs along the eastern side, while to the northeast of the town it flows into a deep canyon cut into Holocene lahar deposits and lavas.

At the bottom of the valley, some small topographic heights up to 15 m high are present, composed of horizontal pyroclastic fall deposits laid down on an originally flat morphology. These deposits overlie a sedimentary succession represented by massive conglomerate, fine sand and subordinate clayey deposits of fluvial and lacustrine origin.

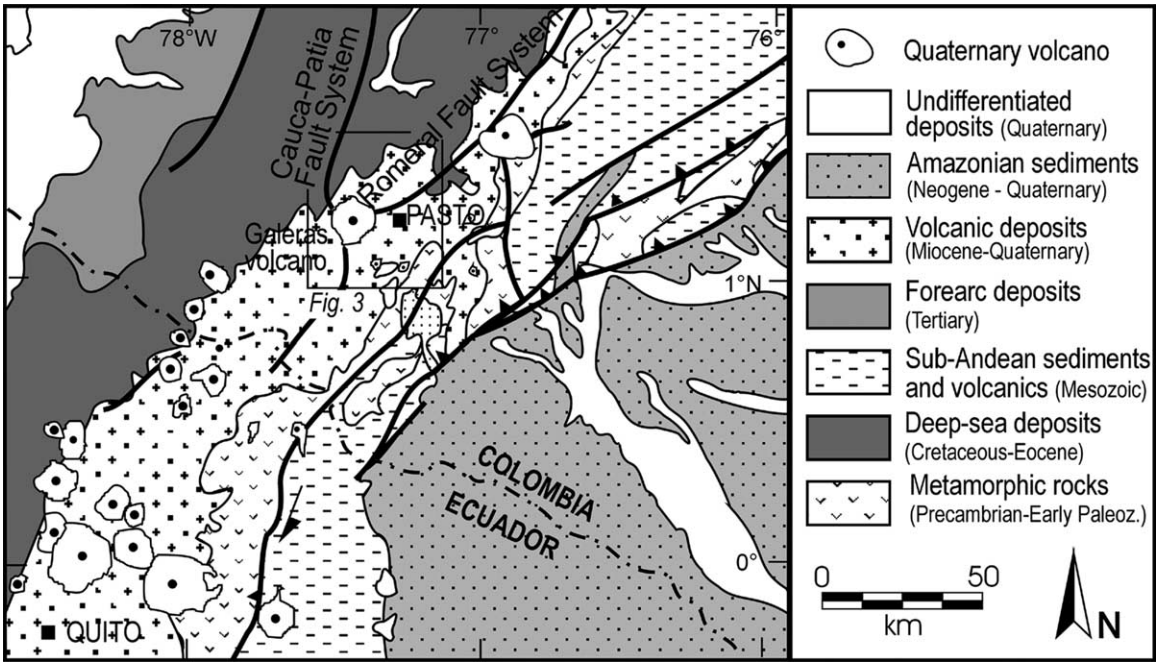

Fig. 2. Regional structures and geology of the area from INGEOMINAS (1988). Location is given in Fig. 1. Box locates Fig. 3.

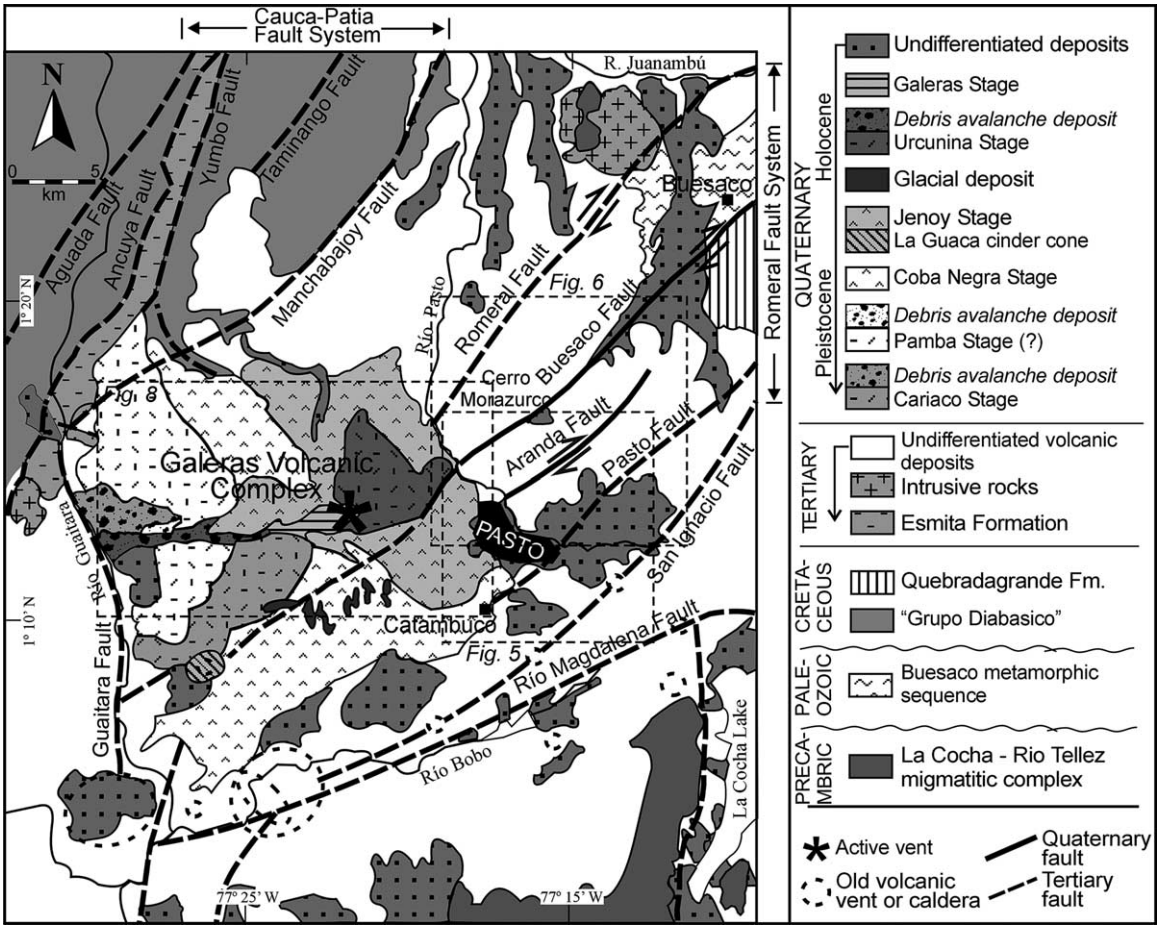

Fig. 3. Main geological units from INGEOMINAS (1991), Calvache et al. (1997) and this work. Note the difference between the structures in this map and those of latest Pleistocene–Holocene age in Fig. 15 resulting from the present work. Location is given in Fig. 2. Boxes locate Figs. 5, 6 and 8.

Another widespread deposit is represented by massive over-consolidated fine volcanic ashes, reworked by aeolian action, locally referred to as 'Cangahua' formation.

The age of this succession is constrained by the radiometric datings available for the Galeras volcano deposits, reported in Calvache et al. (1997) (Fig. 4). In the southern part of the Pasto Valley, the products of the latest explosive activity of the Coba Negra volcanic stage, dated between 793 ± 20 and 288 ± 40 ka BP, crop out. To the west, the valley is limited by the eastern slope of Galeras volcano, composed of the products of the Jenoy stage, dated between 288 ± 40 and 31 ± 0.4 ka BP. The subsequent Urcunina volcanic stage continued its activity until at least 12.8 ± 0.3 ka BP. The deposits from this stage cover a glacially moulded landscape and show no evidence of glacial reworking and thus may be contemporaneous with or younger than the post-Last Glacial Maximum (LGM) glacial retreat in this area, dated at 20–23 ka BP (Seltzer et al., 1995). The fall deposits that constitute the topographic heights at the bottom of the Pasto Valley belong to the sequence of the most recent volcanic stage, named Galeras and dated at <4.5 ka BP. During this stage, the activity of the volcano consisted of six major explosive eruptions that produced lithic-dominated fall and flow deposits. These fall deposits overlie the fluvial and lacustrine sequence described above, giving it an age older than 4.5 ka BP. Since the valley is lower than the minimum altitude reached by Holocene glaciers in the Andes of Colombia (3000–3500 m; Thouret et al., 1997), this sedimentary sequence can be ascribed to fluvial and lacustrine deposition in a periglacial environment during the LGM (20–23 ka BP) or immediately after it.

3. Main late Pleistocene–Holocene faults around Pasto

In order to study the features of recent faulting in the area around Pasto, aerial photo interpretation was coupled with field stratigraphic, structural and morphological data. Morphometric analysis (Peltzer et al., 1988; Tibaldi and Romero, 2000) and fault plane tectoglyphes have been used to characterise the fault kinematics. We describe three main faults (length ≥ 6 km; Fig. 5), the already known Buesaco and Aranda Faults (Tibaldi and Romero, 2000), the newly

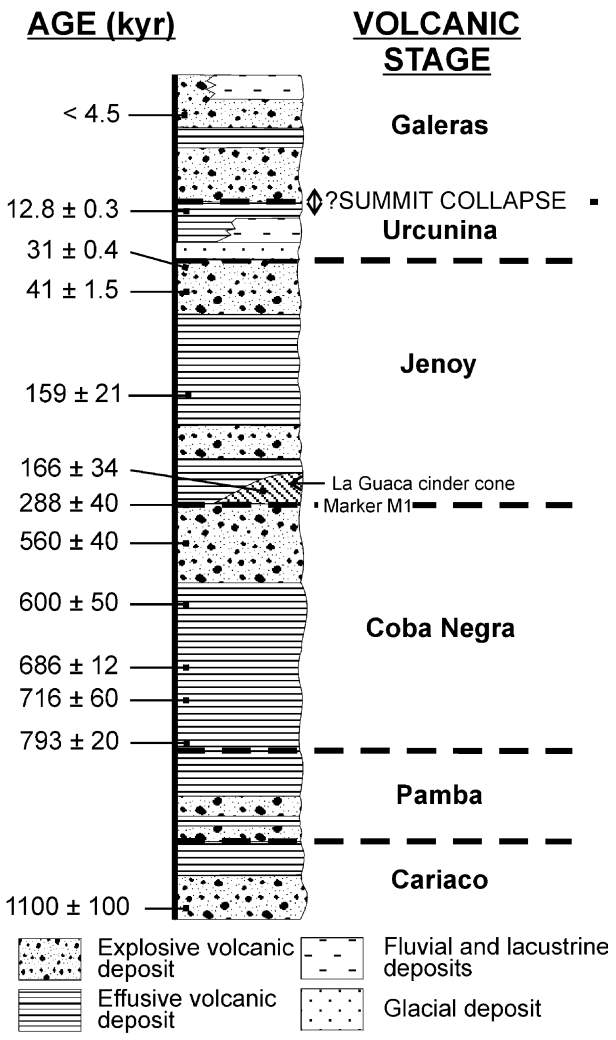

Fig. 4. Stratigraphy of the deposits cropping out in the valley of Pasto and its surroundings from field survey of the authors and from Calvache et al. (1997).

recognized Pasto Fault, and 21 secondary faults (length < 6 km) all with evidence of latest Pleistocene–Holocene motions.

The Buesaco Fault is part of the Romeral Fault System (Figs. 3 and 5). Its 29-km-long trace extends from the lowermost eastern slope of Galeras to a few kilometres NE of the town of Buesaco. To the SW, the fault strikes ENE and then bends to the NE (Fig. 6). Farther NE, two parallel fault traces, 200–400 m apart, form a small pull-apart basin, following which a single NE-striking fault trace is present. The fault trace makes a clear break in slope across the foothills with fault scarps that face either to the NW or the SE, depending on the orientation of the topography with respect to the fault trace, suggesting dominant strike-slip motions. Gullies and ridges crossed by the fault are systematically displaced right-laterally. Flat swampy depositional areas have formed where drainage is dammed by uphill facing fault scarps. Based on relationships between the topography and the fault trace, it is inferred that the fault plane is vertical.

The Aranda Fault crosses the SE slope of Cerro Morazurco at an altitude of 2600–3200 m (Figs. 3 and 6). The fault trace is visible from the NE edge of Pasto to a few kilometres south of Villa Moreno with a length of 13 km. It strikes ENE near Pasto and then bends to the NE. The trace of the Aranda Fault makes a clear break in the slope with the same evidence of dominant strike-slip offset as the Buesaco Fault. The relationships between the topography and the fault trace indicate a vertical plane. From the field measurements of horizontal and vertical components of surface fault offset, the average pitch plunges 2.5°±0.5° to the WSW along the central-southern part of the fault. Farther north, the reconstructed pitch plunges 7.1°–8.4° to the WSW. All segments of the Aranda Fault trace are thus consistent with a WSW-plunging pitch and a slight uplift of the northwestern block (Tibaldi and Romero, 2000).

The Pasto Fault is located a few kilometres to the southeast of the Aranda Fault (Figs. 3 and 6). The evidence of recent movements of the Pasto Fault extends from the eastern edge of the town to about 11 km NE. The fault strikes NE and has a rectilinear trace in plan view. Fault scarps face either NW or SE, depending on the orientation of the topography with respect to the fault, but show lower slope angles than the other two faults. Most of the landforms crossed by the fault are systematically displaced, indicating clear right-lateral strike-slip motions (e.g. Fig. 7B and C). No vertical component of offset is present. The relationship between topography and the fault trace suggests that the fault plane is vertical.

Some faults affect the Galeras edifice. On its south-western slope, ENE- to E-striking faults create a 1.5-km-wide and 7.5-km-long fault swarm from the Cerro La Guaca pyroclastic cone to the Telpis Lake (Fig. 8). Each fault

Table 1
Amount of slip measured along the Buesaco, Aranda and Pasto Faults and slip-rates computed for the three faults. Long- and short-term slips, respectively, refer to Pleistocene–Holocene and Holocene morphological features. Data from the Buesaco and Aranda faults are from Tibaldi and Romero (2000)

	Long-term slip (m)			Short-term slip (m)			Slip-rate (mm/yr)	
	Horizontal	Vertical	Net	Horizontal	Vertical	Net	Long-term	Short-term
Buesaco Fault	188.0±14.0	48.3±3.3	199.6±17.8	2.9±0.9	3.0±0.2	4.2	1.48±0.12	0.65±0.05
Aranda Fault	160.1±11.0	–	160.1±11.0	48.0±13.0	3.9±1.9	48.5±6.5	1.19±0.08	2.30±0.30
Pasto Fault	392.0±25.0	–	392.0±25.0	97.0±9.0	–	97.0±9.0		

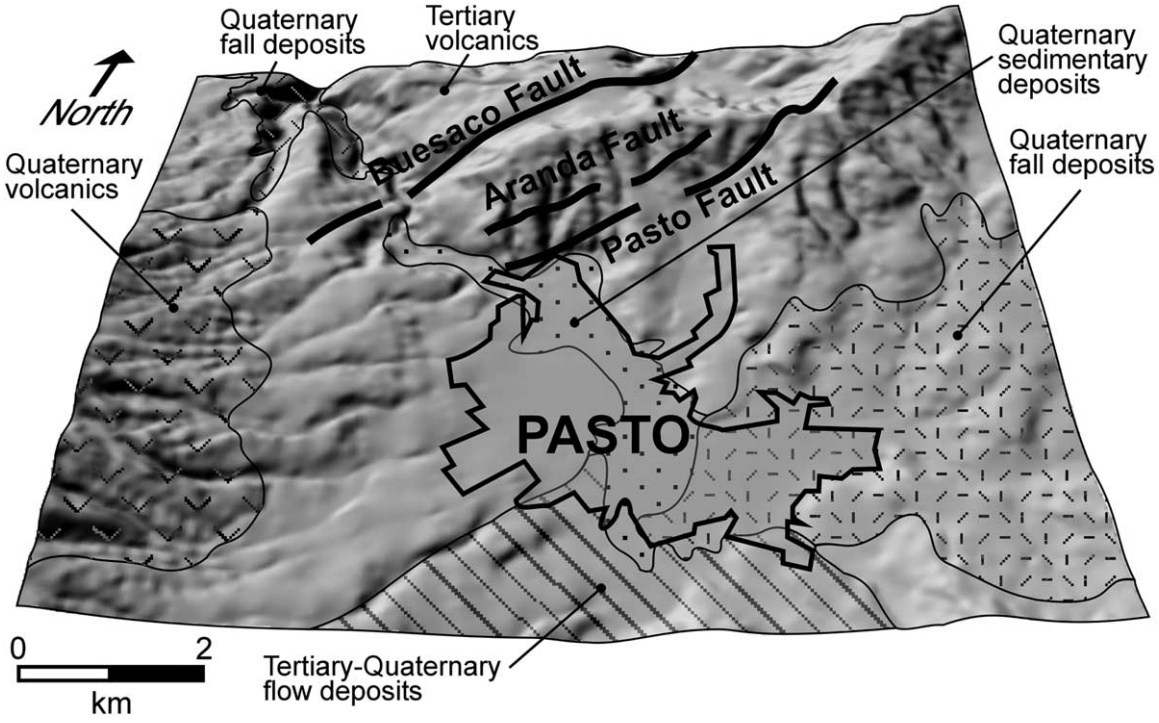

Fig. 5. Geology and morphology of the Pasto Valley. Latest Pleistocene–Holocene main faults around the town and geology are also represented. Location is given in Fig. 3.

segment has a length of 1–2 km and an offset of <10 m. These fault segments displace an erosional surface of glacial origin. On the NW slope of Galeras, two parallel NE-striking faults offset volcanic deposits belonging to the Coba Negra and Pamba volcanic stages. The northwesternmost fault is 5 km long and has a dominant vertical offset of 10–20 m with relative downthrow of the SE block, while the other fault is 2 km long. The rectilinear trace in plan view suggests a vertical dip.

Tibaldi and Romero (2000) described the latest Pleistocene–Holocene activity of the Buesaco and Aranda Faults by means of morphometric analysis and cross-cutting relationships with recent deposits and landforms. The age of these landforms was defined by correlating them with both the available absolute ages of deposits and the main phases of erosion and deposition inferred from different climatic records at a regional scale.

The amount of offset varies along each of the three main faults, with the older topographic features showing greater displacement. In this way, the measured offsets cluster in two different ranges, defining the long- and short-term cumulative slip, respectively referred to Pleistocene–Holocene and Holocene morphological features. Horizontal offset measurements were first obtained from the correlation of two topographic profiles levelled parallel to the fault traces on each side of the fault (Peltzer et al., 1988) and obtained from 1:10,000 topographic maps. Then the obtained offset values were checked in the field by directly measuring, wherever possible, the offset between displaced landforms, such as gullies and crests. Horizontal, vertical and net displacements measured along the three main faults are reported in Table 1, together with their errors. The errors indicate uncertainty in field measurements and correspond to the uncertainty in the projection of the non-rectilinear morphological features to the fault trace (Tibaldi and Romero, 2000).

In order to compute the slip-rates of the main faults, the obtained offset values were divided by the age of the related deposit or landform. The ages were obtained from the available radiometric dating of deposits or deduced from the correlation with the main phases of erosion and deposition inferred from different climatic records at a regional scale (Tibaldi and Romero, 2000; Rovida, 2001). Given the altitude of the studied area and the evidence of past glaciations, the main phases of morphological modelling may have occurred in the last interglacial and postglacial periods, as a consequence of fluvioglacial erosion. Periods of enhanced water runoff followed the last two main glaciations, occurred at a regional scale in the interval 159–41 ka, followed by another phase <41 ka. An older glacial event can be identified immediately before the beginning of the last interglacial period that occurred 120–135 ka (Lanbeck and Nakada, 1992). The interglacial period was then followed by the LGM (20–23 ka; Seltzer et al., 1995),

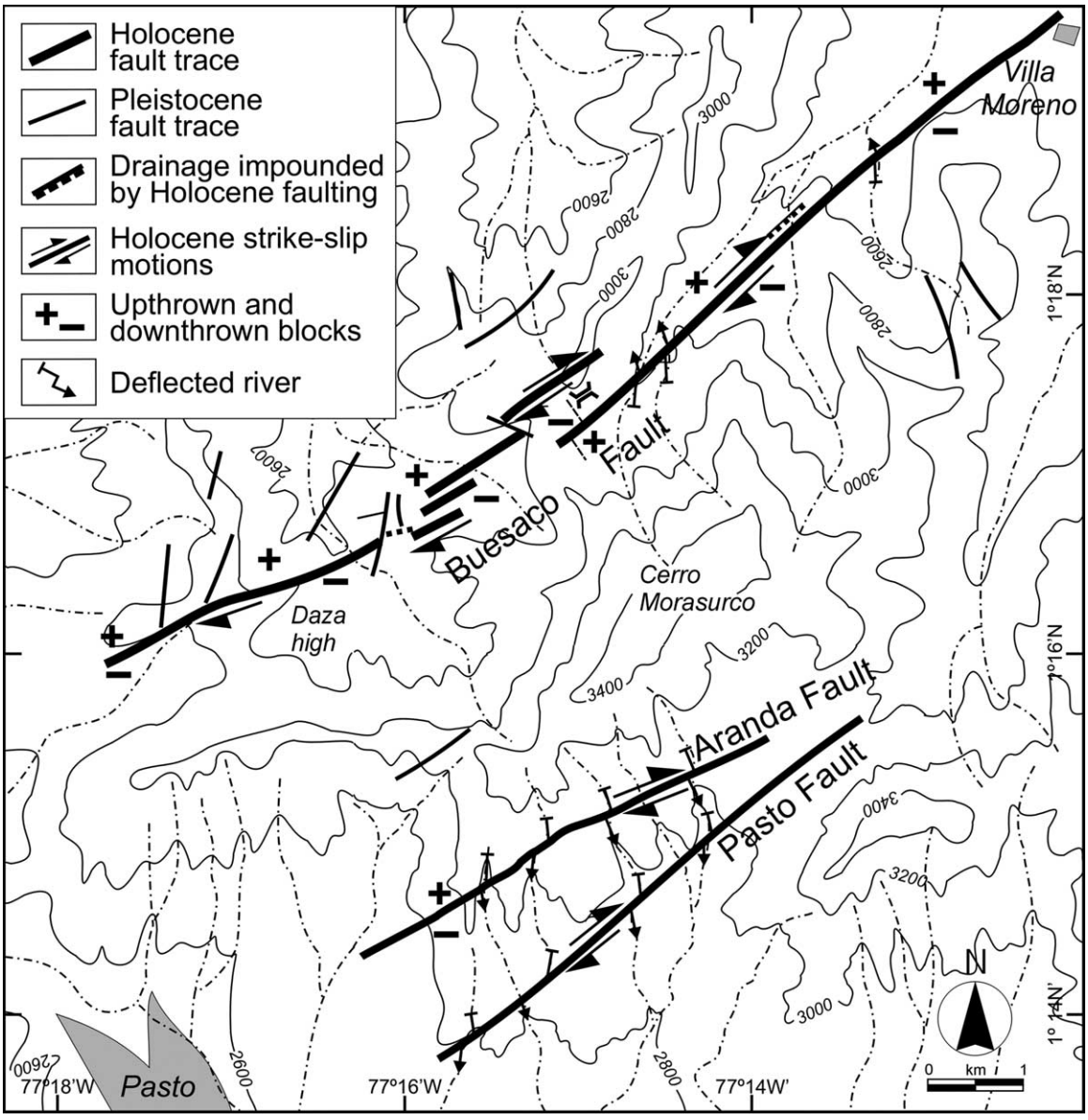

Fig. 6. Map of the surface expression of the Buesaco, Aranda and Pasto Faults with evidence of latest Pleistocene–Holocene offset. Location is given in Fig. 3.

followed by a considerable glacial retreat in central Colombia at 21 ka (Thouret et al., 1997). Deglaciation is correlated with the rapid global warming that marked the onset of the present postglacial period with a rapid sea level rise in the interval 14–11.5 ka (Fairbanks, 1989; Bard et al., 1990). This was generally followed by an increase in pluvial runoff with vigorous erosion during the early Holocene, in the interval 8–6 ka. Tibaldi and Romero (2000) thus consider that the main periods of morphological modelling should have occurred in the intervals 135–120 and 21–6 ka, with postglacial fluvial sedimentation being at a maximum during 8–6 ka. Thus, referring the measured long- and short-term offset, respectively, to the 135–120 and 21–6 ka time intervals, the long- and short-term slip-rates reported in Table 1 were defined. The short-term slip-rate for the Buesaco Fault was computed referring the 4.2 m offset of an alluvial fan (Fig. 7A) to the period of enhanced fluvial sedimentation at 8–6 ka.

Recent activity of the faults themselves is also testified by the occurrence of several shallow, moderate to strong seismic events reported in the area by both historical and instrumental catalogues (CERESIS, 1985; INGEOMINAS, 2002). Historical earthquakes with epicentral intensity $I_0 >$ VII that produced severe damage to the town of Pasto were reported in 1834, 1926, 1933, 1935, 1936, 1947 and 1974, while instrumental, lower energy (mb = 4.4–5.3) events happened in 1985, 1995 and 2000 (INGEOMINAS, 2002).

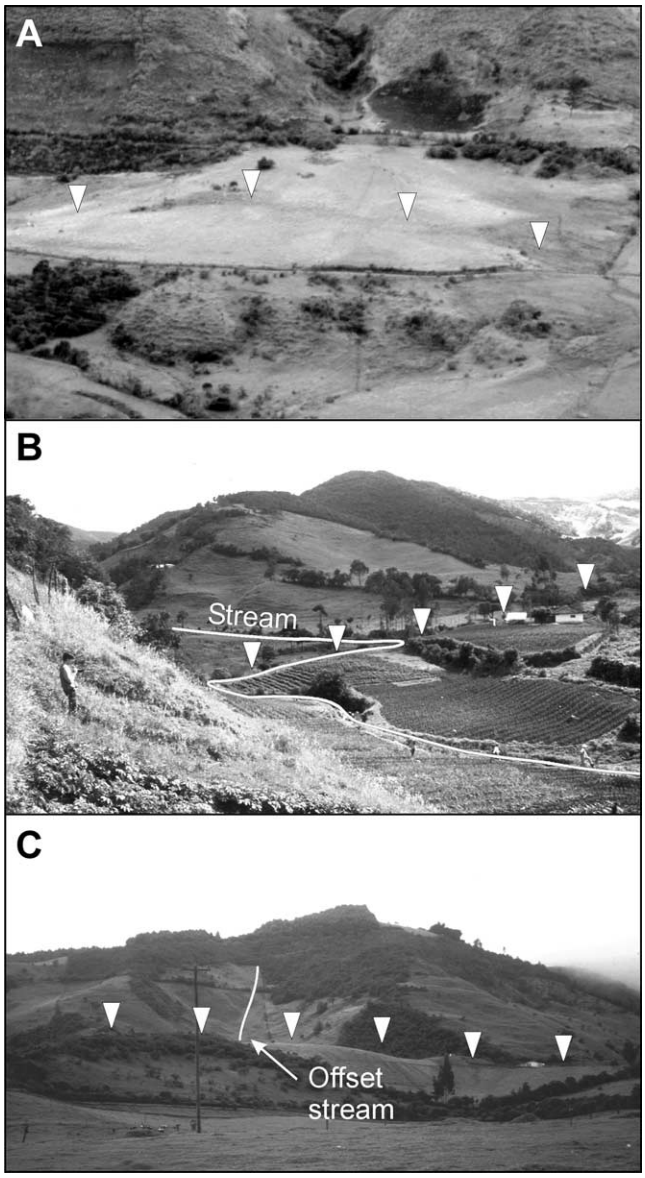

Fig. 7. (A) Alluvial fan affected by the Buesaco Fault. (B) Right-lateral transcurrent deflection of a small river along the Pasto Fault. Person for scale. (C) Example of no correspondence of landforms on the two tectonic blocks separated by the Pasto Fault.

The epicentres of these events are located both to the SW and to the NE of Pasto and follow a NE–SW direction (Fig. 9), consistent with the strike of both the main faults in the study area and the regional structures. The most recent important earthquake occurred on 4th March 1995 with a local magnitude MI = 5.1 and was localized 20 km north of the town on the prolongation of the Buesaco Fault with a focal depth of 11 ± 5 km (INGEOMINAS, 1995). The focal mechanism solution obtained for this earthquake shows right-lateral strike-slip kinematics along a nodal plane striking N053° and dipping 73° to the NW (INGEOMINAS, 1995), consistent with the geometry and kinematics of the Buesaco Fault as observed in the field.

4. Holocene structures within Pasto

Structural data were also collected at 12 sites in the urban area of Pasto and its surroundings (Fig. 10). These sites are mostly located in stream channels, road cuts or in some of the quarries present in the town suburbs. The study also benefited from the giant excavation for the construction of a new sports stadium, with several outcrops of both the sedimentary succession and the pyroclastic fall and flow deposits. The volcanic products mostly belong to the upper part of the Galeras Volcano sequence, namely the late Urcunina and Galeras volcanic stages, with an age younger than 12.8 ± 0.3 ka BP (Calvache et al., 1997). At Catambuco (site no. 8 in Fig. 10) on the other hand, the succession dates back to the youngest products of the Coba Negra stage, with a pyroclastic flow deposit dated 560 ± 0.4 ka BP (Calvache et al., 1997). At Quebrada El Chorillo (site no. 9, Fig. 10) the outcropping succession belongs to the upper part of the Jenoy stage, with the lowermost pyroclastic fall deposit dated 41.0 ± 1.5 ka BP (Calvache et al., 1997).

The outcrops investigated expose widespread fractures. The term *fracture* is used as a general term for any observed discontinuity, with no reference to either extension or shear displacement. With the term *joint* we refer to fractures with no evidence for displacement parallel to the walls, and are either open or filled. The term *microfault* is used to refer to brittle failure structures showing millimetre to centimetre shear displacement. This displacement was observed at the intersection with other fractures or it was inferred from the presence of striated planes, rarer tectoglyphes represented by steps on the fault plane deriving from the intersection between P and R fractures and the principal plane (Petit, 1987), and thin patinas of micro-cataclasite. Only the fractures affecting at least two depositional units have been considered, in order to discriminate between tectonic structures and those produced by the cooling of volcanic products or by compaction phenomena. Moreover, fracture planes close and parallel to slopes were not considered because of their possible gravitational origin.

About 300 fracture data were collected (Fig. 10) and they can be grouped into two main sets, strike-slip microfaults ($n = 44$) and joints ($n = 233$).

The microfaults mostly show right-lateral strike-slip displacement on N030°–N100° (mode N065°) striking planes and very subordinately left-lateral strike-slip offset on N115°–N120° striking planes (Fig. 11). The same graph of Fig. 11 shows that all of them are steeply dipping (> 75°). The stress tensor, calculated by striae pitch and orientation of microfault planes inversion ('Dièdres droits' method; Angelier and Mechler, 1977) shows a horizontal maximum principal stress (σ_1) trending ~N060° and a horizontal minimum principal stress (σ_3) trending ~N150° (Fig. 11). Microfaults affect only the outcrops located on the slopes of the Pasto Valley and are absent elsewhere (Fig. 10).

All the observed joints show offset in the order of millimetres perpendicular to the joint plane, suggesting that they are dilation (Mode I) fractures (e.g. in Fig. 12). Their

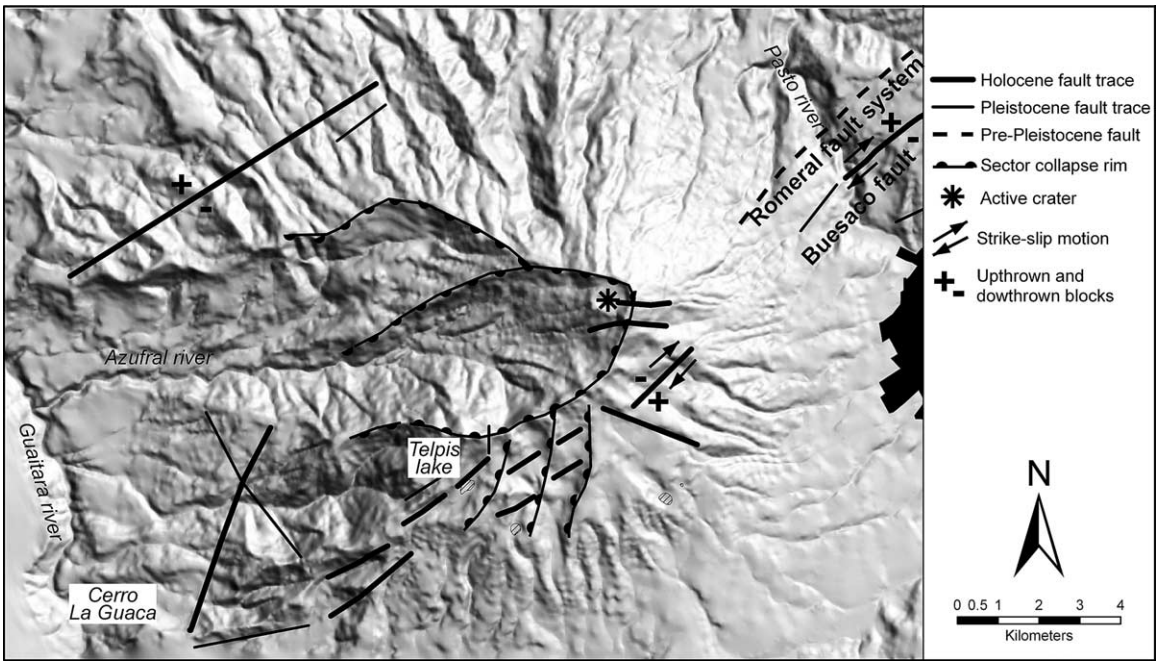

Fig. 8. Main recent structures on the flanks of the Galeras Volcano. All these faults strike NE with the exception of a few structures located near the summit of the edifice, which strike about E–W.

strike is dispersed but presents peaks around a N–S direction, N065° and N020° in decreasing order of frequency (Fig. 13). Their dip ranges from 45° to vertical, with a modal dip of 85°. Some ($n=23$) of these joints are 1–2.5 cm open (Fig. 14) and they are sometimes filled by reworked volcanic deposits or by halloisite (Muñoz, 1998), a clay mineral derived from weathering of volcanic ash. The strike of this subset ranges from N030° to N080°, with a modal strike of N070°, and the prevailing dip direction is towards the SSE–SE (Fig. 13). They are steeply dipping with a modal dip of 75°. The inferred main dilation direction is NNW–SSE (Fig. 13) and it is consistent with the trend of σ_3 obtained from the analysis of microfaults.

Based on all these characteristics, we can describe this structural pattern as a joint spectrum (sensu Hancock, 1986). A joint spectrum is an angular continuum of differently oriented coaxial structures that are dynamically compatible. A complete spectrum comprises a 60° angular range of hybrid (Mode II/III) fractures and dilation (Mode I) fractures (Hancock, 1986). In this perspective, our data suggest that the N–S and N065°-striking joints can be considered as two conjugate sets made up of hybrid and shear joints (Modes II/III). These two sets form opposing dihedral angles that contain the Mode I striking fractures.

These three sets of structures mutually cut each other, suggesting contemporaneous formation. In view of the young age of the fractured deposits, it is likely that all these structures originated under the same stress field.

5. Discussion

5.1. Age, style and amount of deformation around and within Pasto

Brittle deformation processes occurred in the latest Pleistocene and Holocene both in the outcropping rocks around Pasto and within the infill of the Pasto Valley. This deformation resulted in a main NE-trending zone of fracturing and faulting crossing the study area (compare Figs. 3 and 15). Faulting around Pasto has occurred along NE- to ENE-striking vertical planes. Offset landforms, dated 135–120 and 8–6 ka (Tibaldi and Romero, 2000) and some striated fault planes show recent right-lateral strike-slip motion with a very subordinate component of relative upthrow of the northwestern blocks. The largest offsets correspond to the long-term (latest Pleistocene–Holocene) cumulative slip, ranging some tens to hundreds of meters, whereas the smaller values correspond to the short-term (Holocene) cumulative slip, ranging a few metres to tens of metres.

In the Pasto Valley, Holocene brittle deformation occurred along structures with the same dominant NE and ENE strike, but with offset in the order of centimetres. Microfaults and joints affect pyroclastic and sedimentary deposits whose age can be mostly ascribed to the Holocene, being younger than 12.8 ka according to the available radiometric dating (Calvache et al., 1997; Fig. 4). Some of these structures also affect deposits dating back to the late Pleistocene. As with the master faults, these microfaults

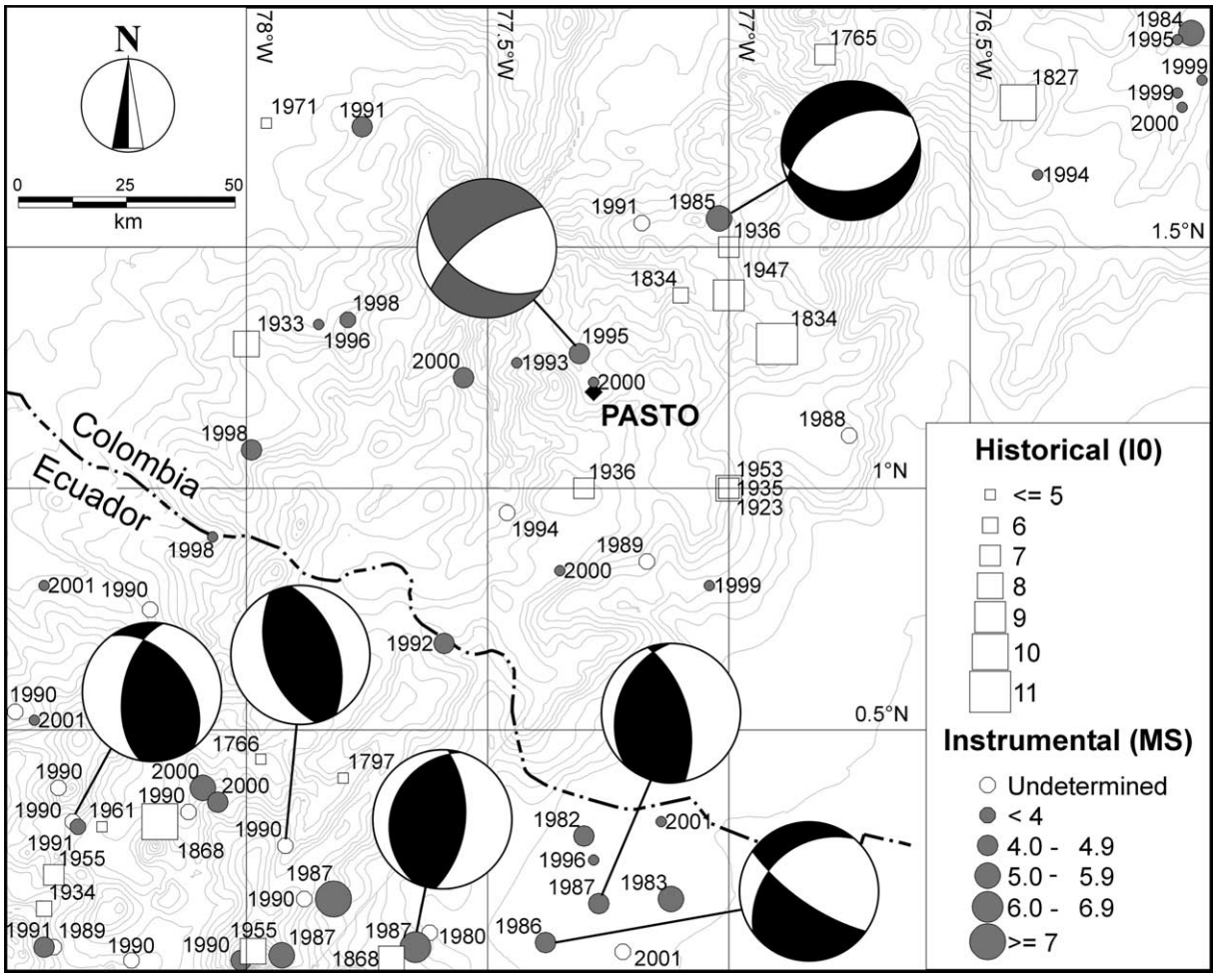

Fig. 9. Epicentres of the historical and instrumental earthquakes of the southern Andes of Colombia from CERESIS (1985) and INGEOMINAS (2002) catalogues. Regional focal mechanism solutions (black) are from Harvard CMT Catalog, the dark grey one refers to the March 1995 earthquake (INGEOMINAS, 1995). Location in Fig. 1.

show right-lateral strike-slip motions and can be interpreted, respectively, as synthetic P and Riedel shears (P and R; Fig. 16). The other main set of microfaults strikes ESE and shows left-lateral strike-slip motions. They can be interpreted as antithetic Riedel shears (R′; Fig. 16), according to classical simple-shear models (e.g. Tchalenko, 1970). Joints have more dispersed strikes than microfaults and are described as a joint spectrum. This contains the ENE-striking dilation joints (T; Fig. 16) whose orientation is consistent both with the acute dihedral angle between the shear and hybrid joints striking NNE to NE and ESE, and with the acute dihedral angle formed by the Riedel shear microfaults. The spectrum of joint orientations may reflect the heterogeneity of the rocks and small changes in values of the effective minimum principal stress (σ'_3) and of the effective differential stress ($\sigma'_1-\sigma'_3$) without any rotations of principal stress axes (Hancock, 1986). The higher range of joint azimuths compared with microfaults supports the idea that within a joint spectrum only those planes presenting suitable orientations can assume the role of shear faults.

The stress tensor obtained by the inversion of the microfault kinematic data shows a horizontal ~N060° trending maximum principal stress (σ_1) and a ~N150° trending minimum principal stress (σ_3). The same extension direction is consistent with the orientation of dilation joints. This same state of stress is consistent with the focal mechanism solution of the 1995 earthquake (Fig. 9), also indicating dominant strike-slip displacement. At a regional scale, other focal mechanism solutions also indicate the presence of a compressional state of stress characterized by a horizontal ENE- to E-trending P axis and a horizontal NNW- to N-trending T axis (Pennington, 1981; Taboada et al., 2000).

In conclusion, the basement outcropping northeast of Pasto and the deposits in the valley show similar and compatible characteristics of deformation, except for the continuous fault planes in the basement with a

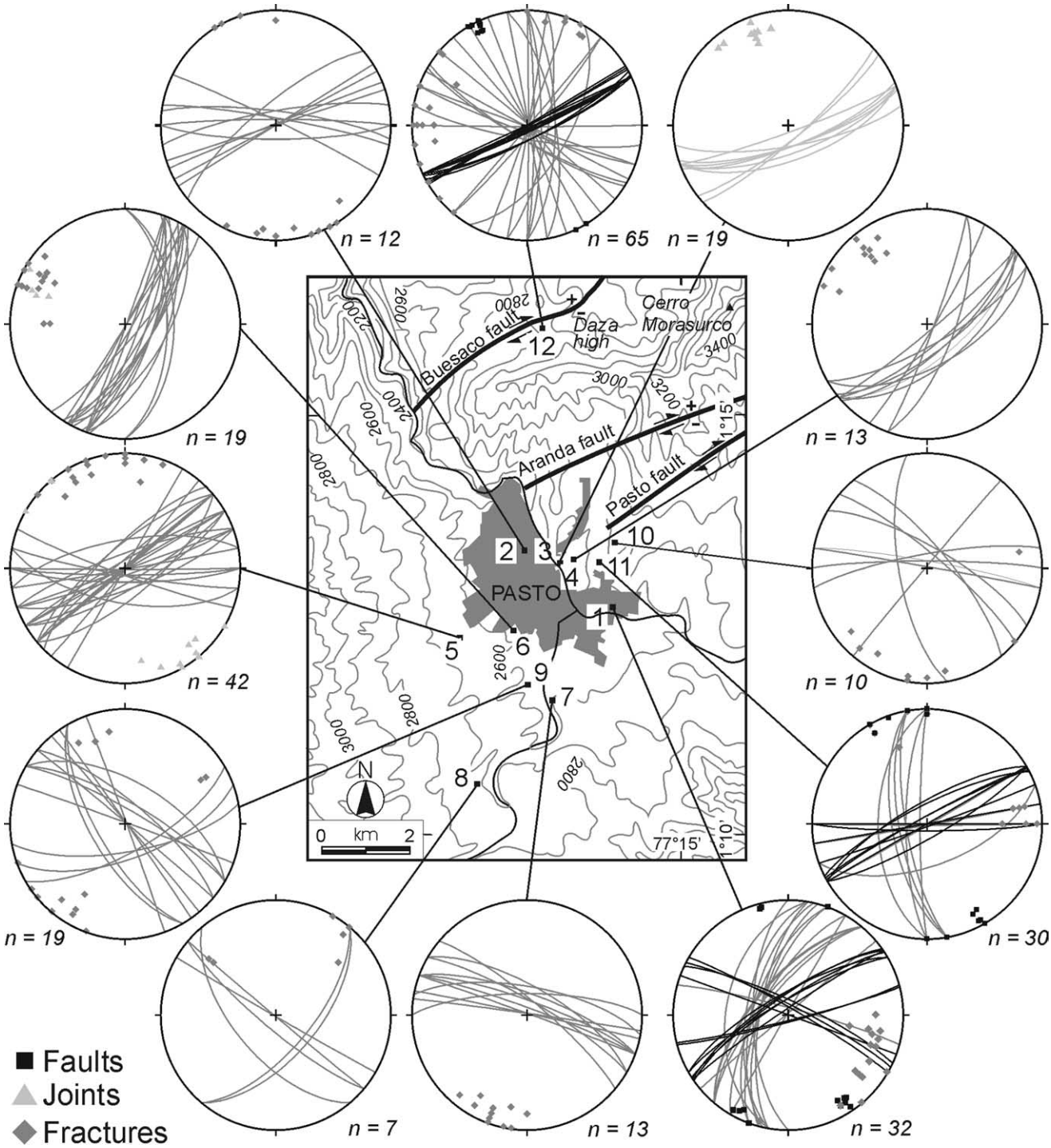

Fig. 10. Structures of Pasto Valley. Schmidt's stereonets represent poles to planes (lower hemisphere). They show the geometry of the various microfaults and joints and the location of measurement.

deformation amount several orders of magnitude higher than elsewhere.

5.2. Possible models for the different amount of deformation

The described zone of simple shear, represented by the master faults affecting the basement and the mesoscale fractures affecting its cover, can be interpreted and genetically explained in terms of a damage zone (e.g. Cowie and Scholz, 1992; McGrath and Davison, 1995; Kim et al., 2004). The development of different structures within damage zones gives valuable information about fault

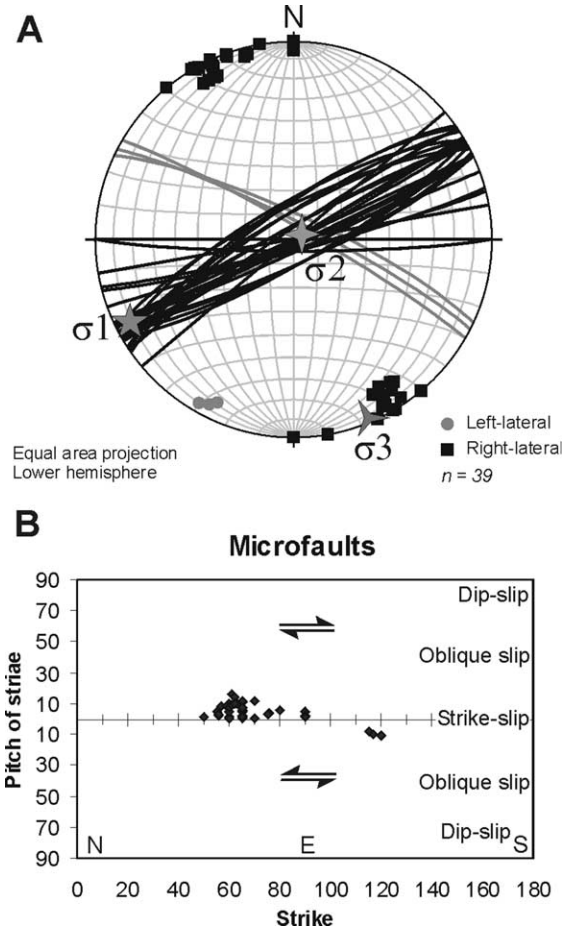

Fig. 11. Diagrams of microfault characteristics measured in the Pasto area. (A) Schmidt's stereonets (lower hemisphere) of the planes. (B) Pitch (*X*-axis) versus strike (*Y*-axis). Most microfaults strike ENE, NE and ESE in decreasing order of frequency. The total number of structures in diagram B is lower than in diagram A because not all the microfaults showed good kinematic indicators.

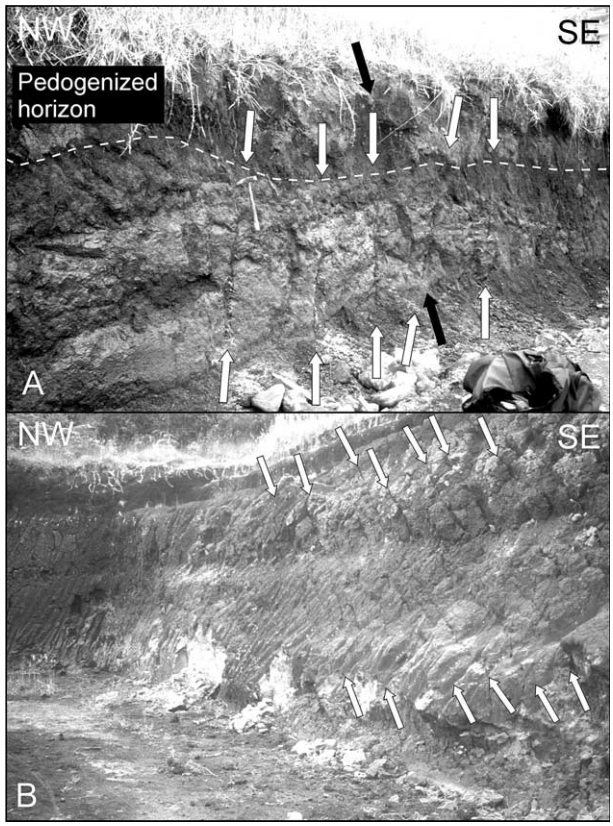

Fig. 12. Photo of NE-striking joints and right-lateral strike-slip microfaults at Pasto (A) and in the surrounding area (B). In (A) most of them (white arrows) are interrupted by the pedogenized horizon, whereas one of them (black arrows) crosses it, testifying an enduring of the fracture process. Hammer for scale.

propagation and growth (McGrath and Davison, 1995; Vermilye and Scholz, 1999; Kim et al., 2003).

The fact that the surface expression of the Aranda and Pasto Faults disappears at the contact between the basement rocks and the young sediments can be explained by two models (Fig. 17):

(1) The main fault planes really end at the contact between the basement and the sedimentary cover in the valley. In this case, the structures affecting the sedimentary cover may be the result of brittle deformation produced by stress propagation at the main strike-slip fault tips (Fig. 17A).
(2) A second model includes the main faults also affecting the basement of the Pasto Valley under the volcano-sedimentary deposits. The slip of the basement faults may have been accommodated by pervasive fracturing and microfaulting in the younger deposits of the valley (Fig. 17B). This may be either due to differing rheological properties of the two materials or to lower strain in the cover.

In both the proposed models, the termination of the main fault traces at the contact between the outcropping basement and its coverage and the observed pattern of fractures affecting the cover suggest the presence of a fault damage zone, according to the definition by Cowie and Scholz (1992), McGrath and Davison (1995) and Kim et al. (2004). This latter paper defines different types of damage zones, based on their position with respect to the master fault and defines as a tip damage zone, the one developed in response to stress concentration at a fault tip. As regards strike-slip faults, two end-member slip modes occur around their tip line. Mode II occurs at the lateral tips and Mode III slip occurs at up- and down-dip tips of the fault. Slip at Mode II tips of a strike-slip fault is commonly accommodated by extension fractures, with dilation at one side of the fault tip and contraction at the other side. The stress distribution at Mode II tips is generally asymmetric across the fault. At Mode III tips of a strike-slip fault, slip generates symmetric stress perturbations, with synthetic and antithetic fractures accommodating slip commonly symmetrically distributed across the fault.

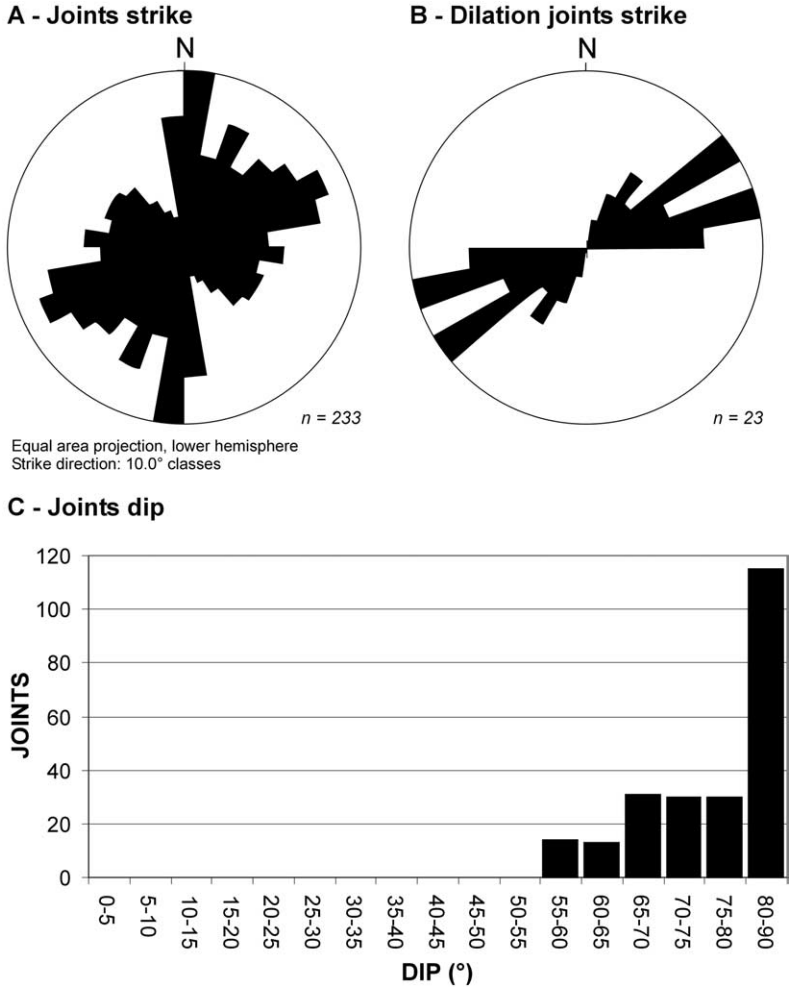

Fig. 13. Diagrams of geometric characteristics of joints and fractures measured in the Pasto area. (A) Azimuths of the total joint population. (B) Azimuths of the dilation joints. (C) 5° dip classes of the total joint population. Dilation joints mostly strike ENE, parallel to the regional trend of the tectonic greatest principal stress.

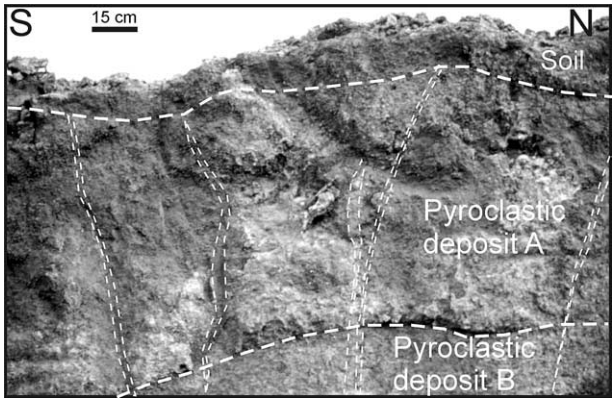

Fig. 14. Outcrop in the western part of Pasto showing a series of ENE-striking dilation fractures. These fractures cross two main pyroclastic deposits (A and B) and are interrupted by the pedogenized horizon. Dilation amount on each fracture is between a few millimetres and 2.5 cm.

According to the two models proposed here, the structures affecting the sedimentary succession of the Pasto Valley may be either the result of brittle deformation produced by stress propagation at the lateral (model 1) or up-dip (model 2) tips of the main strike-slip faults. The features of the structural pattern observed in the Pasto Valley, characterized by microfaults representing antithetic and synthetic shears, respectively, at ~70° and ~20° to the master faults, and extension fractures with the same strike as the regional σ_1 (~N060°), recall the geometry described for Mode III tips of strike-slip faults (Kim et al., 2003) and support the up-dip propagation of the master faults across the sedimentary cover (model 2).

Moreover, model 1 is unlikely as it requires both the two main basement faults to terminate exactly at the contact with the younger deposits. The recent structures with the same NE–SW strike as the Aranda and Pasto Faults are present on the Galeras edifice (Fig. 8) and can represent their continuation beyond the Pasto Valley.

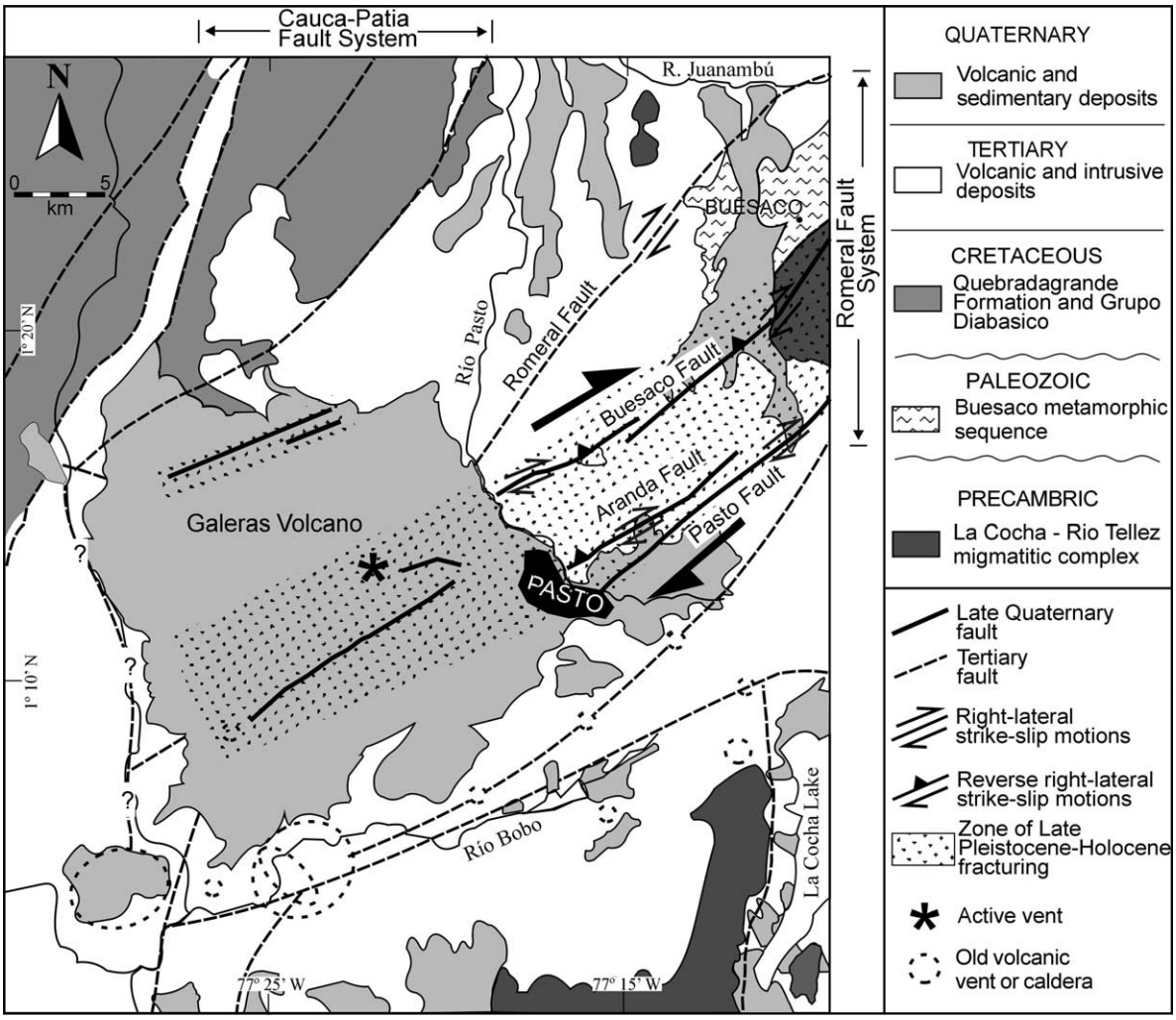

Fig. 15. Latest Pleistocene–Holocene main faults and fracturing–faulting zones resulting from the present work. The area portraying exactly the same as Fig. 3; compare the fault pattern between the two figures.

5.3. Hierarchical shear failure

According to several studies (McGrath and Davison, 1995; Vermilye and Scholz, 1999; Kim et al., 2003), the development of different structures within damage zones gives valuable information about fault propagation and growth. In laboratory experiments, brittle faulting is usually accompanied by dilatancy and microcracking. Microcracking was observed in a variety of rocks, such as granites (Peng and Johnson, 1972; Tapponnier and Brace, 1976; Lockner et al., 1992), sandstones (Dunn et al., 1973; Menendez et al., 1996), conglomerates (Vermilye and Scholz, 1999) and marbles (Olsson and Peng, 1976; Frederich et al., 1989). The formation of localized shear fractures appears to be a progressive process involving the initiation, localization, propagation and coalescence of opening-mode microcracks (Willemse et al., 1997). Pre-existing cracks influence fault localization and growth at the macroscopic field scale (Segall and Pollard, 1983). This study demonstrated that strike-slip faults in granite in the Sierra Nevada nucleated along mineral-filled opening-mode joints formed during a previous deformation event. In our case, by comparison, the young age of the deformed succession in the Pasto Valley shows that the various structures cannot be the result of different tectonic phases following rotation and reorganization of the regional stress field. Moreover, all the regional structural data indicate a persistent stress field during the late Pleistocene–Holocene. Thus, the studied structures developed under the same regional stress field during the Holocene, under the influence of a NE-trending shear zone.

In laboratory experiments, extension fractures formed prior to the nucleation of a fault are sub-parallel to σ_1, whereas those generated in the tip zone make angles of about 20° to the regional σ_1 (Reches and Lockner, 1994; Moore and Lockner, 1995). In our case, joints striking around N065°, parallel to the direction of the regional σ_1, formed first (Fig. 18) and the others developed to

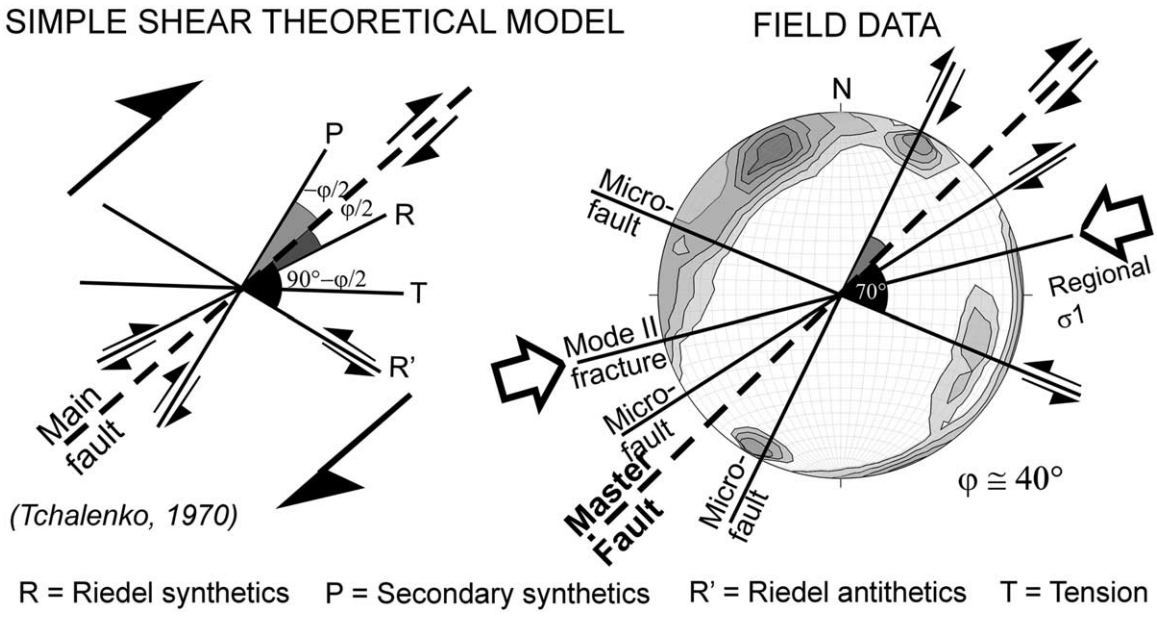

Fig. 16. Comparison between the classical model of secondary faulting along a main wrench fault (left; modified after Tchalenko (19700) and the microfault and joint population in the study area (right). In the study area, right-lateral strike-slip microfaults correspond to synthetic (R) Riedel shears and P structures, whereas left-lateral strike-slip microfaults are antithetic (R′) Riedel shears. NE–SW and WNW–ESE joints represent conjugated shear joints, whereas ENE-striking joints and dilation fractures represent cracks that bisect the opposing dihedral angles between the shear joints. The average angle between the antithetic structures and the main Pasto Fault is $90°-\phi/2$, with $\phi=40°$ for pyroclastic rocks.

accommodate the displacement at a later stage. Then synthetic shear acted along some of these pre-existing joint sets, remobilising preferentially the NE- to ENE-striking set with right-lateral strike-slip motions, whereas NNE-striking joints did not develop into shear structures. To a lesser extent, some of the ESE-striking joints have also been reactivated but with left-lateral strike-slip motions (Fig. 18). In this way, the faulting process developed by nucleation of slip along some of the pre-existing joints. The ENE-striking set of Mode I cracks locally developed into dilation fractures parallel to σ_1. Such a pattern of antithetic and synthetic shears and extensional fractures is typical of the first stage of transcurrent fault development (e.g. An and Sammis, 1996) at the upward propagation of a fault (Mode III tip; Kim et al., 2003).

In succession, most strike-slip motions occurred along the NE-striking planes and subordinately along ENE-striking ones, whereas ESE-striking joints and left-lateral microfaults locked (Fig. 18). This dominance of NE- to ENE-striking fractures, corresponding to synthetic shears associated with the main ENE-striking right-lateral strike-slip faults, is compatible with the known development of a strike-slip deformation zone. In this process, slip along structures that connect incipient boundary fractures is generally synthetic, transferring and connecting slip from one boundary fracture to the next (e.g. Segall and Pollard, 1983).

The distribution of microfaults and joints in the Pasto Valley shows areas of shear concentration. This suggests that shear development is not a diffuse process along all the joints but follows preferred areas since the beginning. In these areas localization of shear is followed by propagation and coalescence of shear planes, whereas in the conterminous areas the joints are not reactivated. In this way, displacement is progressively localized on the major faults (Martel et al., 1988). Our data support the concept that strike-slip planes at the macro-scale can originate from cracking formed both as Mode I and II joints.

6. Conclusions

Based on the field data presented regarding the geometric, kinematic and temporal relations between structures that represent, at different scales, the same deformation pattern, the following main conclusions can be drawn:

(1) Northeast of Pasto, where the master NE- to ENE-striking faults crop out, various increments of river deflection indicate repeated episodes of surface right-lateral strike-slip motions during the latest Pleistocene–Holocene.
(2) Structural and morphological evidence suggests that these faults are also present in the basement below the volcano-sedimentary sequence of the Pasto Valley.
(3) During the Holocene, increments of faulting under the same regional stress field produced brittle failure in the deposits of the Pasto Valley. This failure resulted in a spectrum of open (Mode I) and shear (Modes II/III) cracks.
(4) Mode I fracture orientation is perpendicular to the

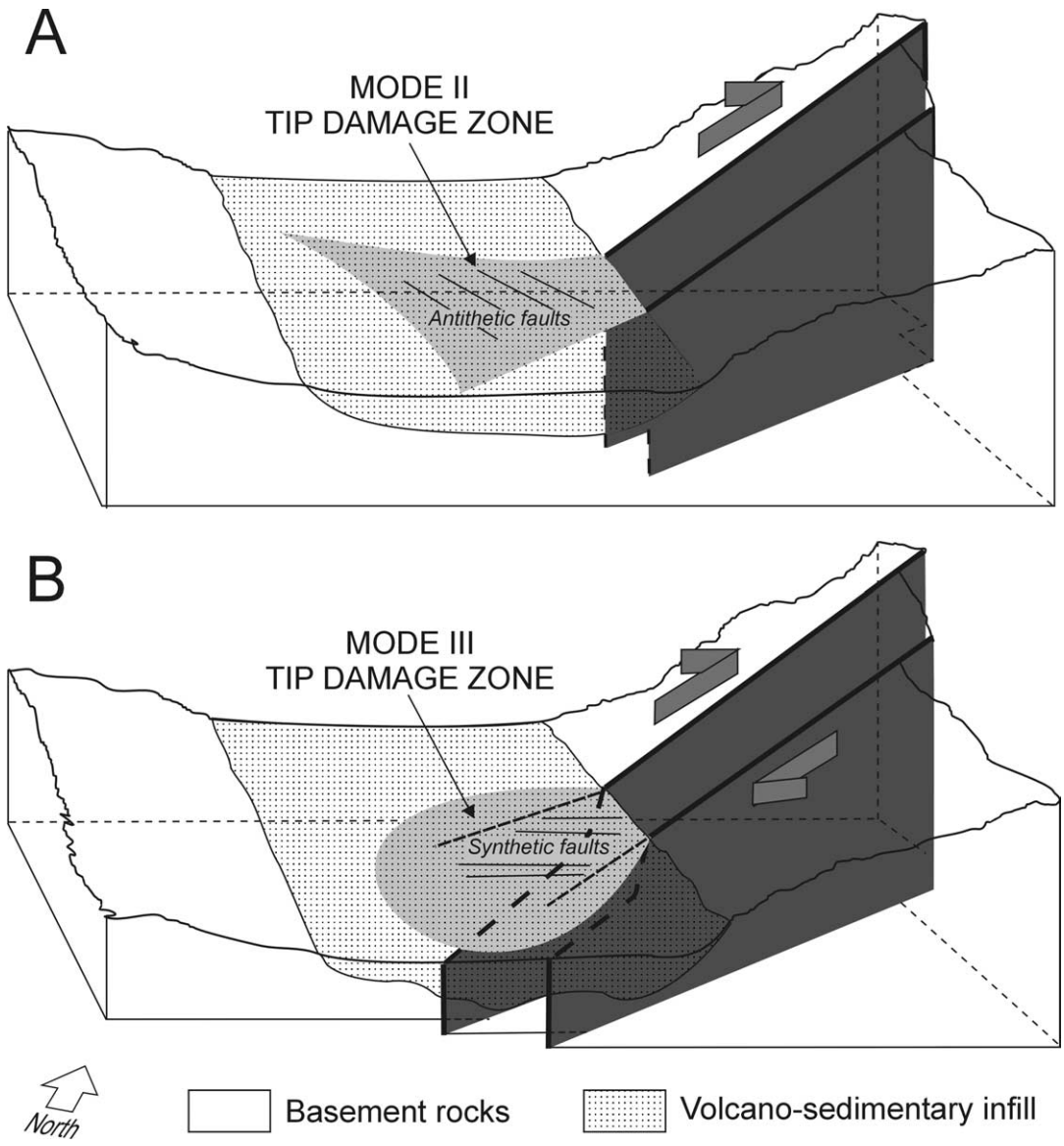

Fig. 17. Models of explanation of the difference of offset amount between the faults cropping out NE of Pasto and the microfaults within the Pasto Valley. In (A), the basement faults die out exactly in correspondence with the boundary of the Pasto Valley infill. In (B), the main basement faults are also present under the volcano-sedimentary deposits of the Pasto Valley with Holocene large faulting occurring only within the basement rocks.

regional minimum principal stress (σ_3), as deduced from the large-scale structures observed in the field, from earthquake focal mechanism solutions and from the stress tensor reconstructed by the analysis of striated fault planes. The associated maximum principal stress (σ_1) bisects the dihedral angle between the Mode II cracks striking NE and those striking ESE.

(5) The faulting process started by nucleation of slip along the synthetic NE-striking shears, accompanied by dilation along the ENE-striking T fractures. Spread of faulting also involves local shear reactivation of the ENE-striking tension cracks.

(6) Our data support the idea that strike-slip fault planes can originate from cracking at the macro-scale; they initiate as multiple set Mode I and II joints, followed by nucleation of slip and connection between the synthetic shear joints.

Acknowledgements

We wish to thank Derek J. Rust and David J. Sanderson for their very useful reviews. Field co-operation with C. Corazzato, J.A. Osorio and J.A. Romero at the Pasto Fault is strongly acknowledged. This study was partly supported by Consiglio Nazionale delle Ricerche and MIUR-FIRB (Italy) and ILP project grants to A.T. The INGEOMINAS

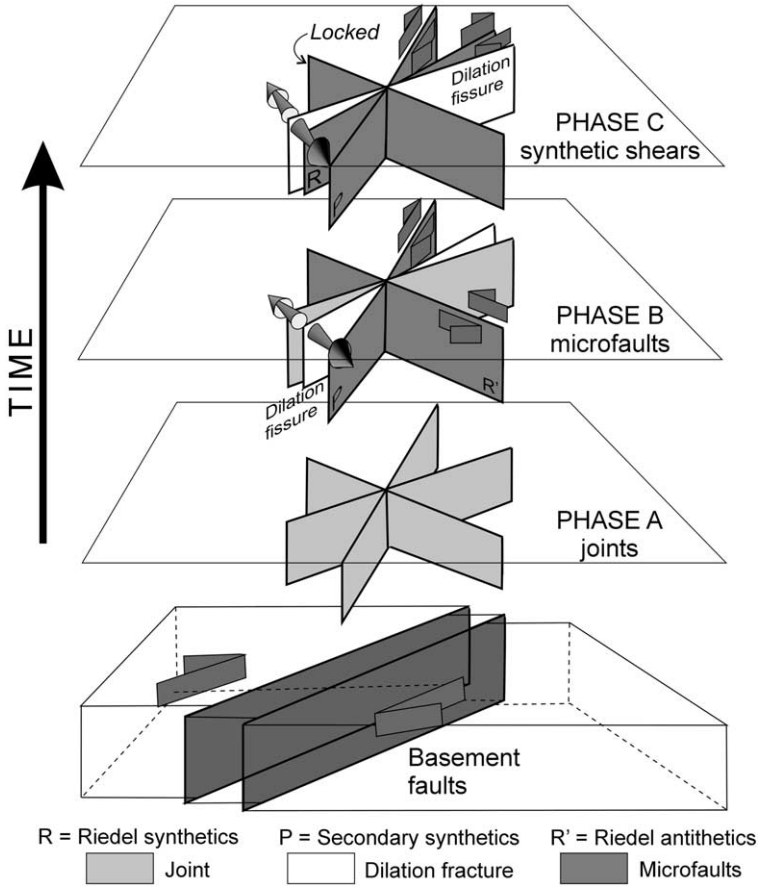

Fig. 18. Sketch of the hierarchical evolution of the structures in the study area above the basement transcurrent faults. (A) Mode II joints striking NNE to NE and ESE, and Mode I joints striking ENE were firstly formed. (B) Some of them, striking NE, have been re-mobilized with right-lateral strike-slip motions as Riedel synthetic shears (R), and those striking ESE with left-lateral strike-slip motions as Riedel antithetic shears (R′). Faulting process developed by nucleation of slip along these pre-existing joints. The ENE-striking set of Mode I cracks developed into dilation fissures parallel to σ_1. Successively (C), most transcurrent motions occurred along the NE-striking planes and subordinately along some of the ENE-striking planes, whereas ESE-striking joints and left-lateral microfaults locked.

Volcanological and Seismological Observatory in Pasto provided the logistical support. This work was carried out in the framework of the UNESCO-IUGS-IGCP Project 455.

References

An, L.-J., Sammis, C.G., 1996. Development of strike-slip faults. Shear experiments in granular materials and clay using a new technique. Journal of Structural Geology 18 (8), 1061–1077.

Angelier, J., Mechler, P., 1977. Sur une method graphique de recherche des constraintes principales également utilisable en téctonique et en séismologie: la method de dièdres droits. Bull. Soc. Géol. France 7, 1309–1318.

Aspden, J.A., McCourt, W.J., 1986. Mesozoic oceanic terrane in the central Andes of Colombia. Geology 14, 415–418.

Bard, E., Hamelin, B., Fairbanks, R.G., Zindler, A., 1990. Calibration of the C14 timescale over the past 30,000 years using mass spectrometric U–Th ages from Barbados corals. Nature 345, 405–410.

Calvache, M.L., Cortes, G.P., Williams, S.N., 1997. Stratigraphy and chronology of the Galeras volcanic complex, Colombia. Journal of Volcanology and Geothermal Research 77, 5–19.

Case, J., Barnes, J., Paris, G., Gonzalez, H., Viña, A., 1973. Trans-Andean geophysical profile, Southern Colombia. Geological Society of America Bulletin 84, 2895–2904.

CERESIS (Centro Regional de Sismología para América del Sur), 1985. Catálogo de terremotos para América del Sur. In: Askew, B. Algermissen, S.T. (Eds). Programa para la mitigación de los efectos de los terremotos en la región andina (Proyecto SISRA). Earthquake Mitigation Program in the Andean Region (Project SISRA). vol. 1–9. http://www.ceresis.org

Cowie, P.A., Scholz, C.H., 1992. Physical explanation for the displacement–length relationship of faults, using a post-yield fracture mechanics model. Journal of Structural Geology 14, 1133–1148.

Cruikshank, K.M., Zhao, G., Johnson, A.M., 1991. Duplex structures connecting fault segments in Entrada sandstone. Journal of Structural Geology 13, 1185–1196.

Dunn, D.E., LaFountain, L.J., Kackson, R.E., 1973. Porosity dependence and mechanism of brittle fracture in sandstones. Journal of Geophysical Research 78, 2403–2417.

Duque Caro, H., 1980. Geotectonica y evolucion de la region noroccidental colombiana. Geotectonics and evolution of the northwestern Colombian region. Boletin Geologico 23 (3), 3–37. INGEOMINAS Bogotà (in Spanish).

Engelder, T., 1989. Analysis of pinnate joints in the Mount Desert Island granite: implications for post-intrusion kinematics in the coastal volcanic belt, Maine. Geology 17, 564–567.

Fairbanks, R.G., 1989. A 17,000-year glacio-eustatic sea level record: influence of glacial melting rates on the Younger Dryas event and deep-ocean circulation. Nature 342, 637–642.

Frederich, J.T., Evans, B., Wong, T.F., 1989. Micromechanics of the brittle to plastic transition in Carrara Marble. Journal of Geophysical Research 94, 4129–4145.

Hancock, P.L., 1985. Brittle microtectonics: principles and practice. Journal of Structural Geology 7, 269–276.

Hancock, P.L., 1986. Joint Spectra. From: Geology in the Real World—The Kingsley Dunham Volume. The Institution of Mining and Metallurgy (Publisher), London, UK, pp. 155–164.

Hancock, P.L., Barka, A.A., 1987. Kinematic indicators on active normal faults in western Turkey. Journal of Structural Geology 9, 573–584.

INGEOMINAS (Instituto de Investigaciones y Informacion Geocientifica Minero Ambiental y Nuclear), 1988. Mapa geologico de Colombia, 1: 500,000 scale, Bogotá, Colombia.

INGEOMINAS (Instituto de Investigaciones e Informacion Geocientifica Minero Ambiental y Nuclear), 1991. Mapa geologico escala 1:100,000, Plancha 429—Pasto, Bogotá, Colombia.

INGEOMINAS (Instituto de Investigaciones e Informacion Geocientifica Minero Ambiental y Nuclear), 1995. El sismo de Pasto (Nariño) del 4 de Marzo de 1995. Boletin de Sismos 3 (1), 63–70. Bogotá (in Spanish).

INGEOMINAS (Instituto de Investigaciones e Informacion Geocientifica Minero Ambiental y Nuclear), 2002. Base de Datos de sismicidad de Colombia, Red Sismológica Nacional y Red Nacional de Acelerógrafos de Colombia, Bogotá. http://bases4d.ingeominas.gov.

Kellogg, J., Vega, V., 1995. Tectonic development of Panama, Costa Rica, and the Colombian Andes: constraints from global positioning system geodetic studies and gravity. Geological Society of America Special Paper 295, 75–90.

Kim, Y.-S., Peacock, D.C.P., Sanderson, D.J., 2003. Mesoscale strike-slip faults and damage zones at Marsalform, Gozo Island, Malta. Journal of Structural Geology 25, 793–812.

Kim, Y.-S., Peacock, D.C.P., Sanderson, D.J., 2004. Fault damage zones. Journal of Structural Geology 26, 503–517.

Lanbeck, K., Nakada, M., 1992. Constraints on the age and duration of the last interglacial period and on sea-level variations. Nature 357, 125–128.

Lockner, D.A., Byerlee, J.D., Kuksenko, V., Ponomarev, A., Sidorin, A., 1992. Observations of quasistatic fault growth from acoustic emissions. In: Evans, B., Wong, T.-F. (Eds.), Fault Mechanics and Transport Properties of Rock. Academic Press, San Diego, pp. 1–31.

Martel, S.J., Boger, W.A., 1998. Geometry and mechanics of secondary fracturing around small three-dimensional faults in granitic rock. Journal of Geophysical Research 103, 21299–21314.

Martel, S.J., Pollard, D.D., Segall, P., 1988. Development of simple fault zones in granitic rock, Mount Abbot quadrangle, Sierra Nevada, California. Geological Society of America Bulletin 100, 1451–1465.

McGrath, A.G., Davison, I., 1995. Damage zone geometry around fault tips. Journal of Structural Geology 17, 1011–1024.

Menendez, B., Zhu, W., Wong, T.F., 1996. Micromechanics of brittle faulting and cataclastic flow in Berea sandstone. Journal of Structural Geology 18, 1–16.

Moore, D.E., Lockner, D.A., 1995. The role of microcracking in shear-fracture propagation in granite. Journal of Structural Geology 17, 95–114.

Muñoz, I.N., 1998. Estudio geologico detallado del area urbana y suburbana del municipio de Pasto. Trabajo de Grado, Universidad de Caldas, Manizales (in Spanish).

Olsson, W.A., Peng, S.S., 1976. Microcrack nucleation in marble. International Journal of Rock Mechanics and Mining Sciences 13, 53–59.

Paris, G., Romero, J.A., 1994. Fallas activas en Colombia. Boletin Geologico 34 (2/3), 3–25. INGEOMINAS, Bogotà (in Spanish).

Peltzer, G., Tapponnier, P., Gaudemer, Y., Meyer, B., Guo, S., Yin, K., Chen, Z., Dai, H., 1988. Offsets of late Quaternary morphology, rate of slip, and recurrence of large earthquakes on the Chang Ma Fault (Gansu, China). Journal of Geophysical Research (B) 93 (7), 7793–7812.

Peng, S., Johnson, A.M., 1972. Crack growth and faulting in cylindrical specimens of Chelmsford granite. International Journal of Rock Mechanics and Mining Sciences 9, 37–86.

Pennington, W.D., 1981. Subduction of the Eastern Panama Basin and seismotectonics of North Western South America. Journal of Geophysical Research 86 (B11), 10753–10770.

Petit, J.P., 1987. Criteria for sense of movement on fault surfaces in brittle rocks. Journal of Structural Geology 9, 597–608.

Reches, Z., Lockner, D.A., 1994. Nucleation and growth of faults in brittle rocks. Journal of Geophysical Research 99, 18159–18173.

Rovida, A., 2001. Neotettonica in aree urbane: l'esempio di Pasto, Colombia meridionale. MSc Thesis, Università degli Studi di Milano-Bicocca, Milano (in Italian).

Rudnicki, J.W., Rice, J.R., 1975. Conditions for the localization of deformation in pressure sensitive dilatant materials. Journal of the Mechanics and Physics of Solids 23, 371–394.

Segall, P., Pollard, D.D., 1983. Nucleation and growth of strike-slip faults in granite. Journal of Geophysical Research 88, 555–568.

Seltzer, G.O., Rodbell, D.T., Abbott, M., 1995. Andean glacial lakes and climate variability since the last glacial maximum. Bulletin de l'institut Francais d'Etudes Andines 24, 539–549.

Taboada, A., Rivera, L.A., Fuenzalida, A., Cisternas, A., Philip, H., Bijwaard, H., Olaya, J., Rivera, C., 2000. Geodynamics of the northern Andes: subductions and intracontinental deformation. Tectonics 19 (5), 787–813.

Tapponnier, P., Brace, W.F., 1976. Development of stress induced microcracks in Westerly granite. International Journal of Rock Mechanics and Mining Sciences 13, 103–112.

Tchalenko, J.S., 1970. Similarities between shear zones of different magnitudes. Geological Society of America Bulletin 81, 1625–1640.

Thouret, J.-C., Van Der Hammen, T., Salomons, B., Juvigné, E., 1997. Late Quaternary glacial stages in the Cordillera central, Colombia, based on glacial geomorphology, tephra-soil stratigraphy, palynology, and radiocarbon dating. Journal of Quaternary Sciences 12, 347–369.

Tibaldi, A., Romero, J.L., 2000. Morphometry of Late Pleistocene–Holocene faulting and volcano–tectonic relationships in the southern Andes of Colombia. Tectonics 19 (2), 358–377.

Vermilye, J.M., Scholz, C.H., 1999. Fault propagation and segmentation: insight from the microstructural examination of a small fault. Journal of Structural Geology 21, 1623–1636.

Willemse, E.J.M., Peacock, D.C.P., Aydin, A., 1997. Nucleation and growth of strike-slip faults in limestones from Somerset, UK. Journal of Structural Geology 19, 1461–1477.